SPIE Proceedings:
GALI a Gamma-ray Burst Localizing Instrument

Roi Rahin[a], Luca Moleri[a], Alex Vdovin[a], Amir Feigenboim[a], Solomon Margolin[a], Shlomit Tarem[a], Ehud Behar[a], Max Ghelman[b], and Alon Osovizky[b]

[a]Department of Physics, Technion, Haifa, Israel
[b]Nuclear Research Center Negev, Israel

ABSTRACT

The detection of astrophysical Gamma-Ray Bursts (GRBs) has always been intertwined with the challenge of identifying the direction of the source. Accurate angular localization of better than a degree has been achieved to date only with heavy instruments on large satellites, and a limited field of view. The recent discovery of the association of GRBs with neutron star mergers gives new motivation for observing the entire γ-ray sky at once with high sensitivity and accurate directional capability. We present a novel γ-ray detector concept, which utilizes the mutual occultation between many small scintillators to reconstruct the GRB direction. We built an instrument with 90 $(9\,\mathrm{mm})^3$ CsI(Tl) scintillator cubes attached to silicon photomultipliers. Our laboratory prototype tested with a $60\,\mathrm{keV}$ source demonstrates an angular accuracy of a few degrees for ~ 25 ph cm^{-2} bursts. Simulations of realistic GRBs and background show that the achievable angular localization accuracy with a similar instrument occupying 1l volume is $< 2°$. The proposed concept can be easily scaled to fit into small satellites, as well as large missions.

Keywords: Gamma-ray bursts, scintillators, silicon photomultipliers, directional gamma-ray detector, small satellites, detector simulations

1. INTRODUCTION

1.1 Astrophysical Context

Astrophysical γ-ray Bursts (GRBs) are the most remarkable transient phenomena in high-energy astrophysics. Long GRBs, those lasting more than 2 s, are generally associated with supernovae, the explosion following the collapse of massive stars. Short GRBs, lasting less than 2 s, are associated with the coalescence of a neutron stars binary,[1,2] and could also result from a merger of a NS and a black-hole binary.[3]

Following the first discoveries of gravitational waves (GWs) from compact stellar mergers by Advanced LIGO (Laser Interferometer Gravitational-wave Observatory), the astrophysics community has concentrated its efforts on detecting their electromagnetic (EM) counterparts. The first direct detection of GWs by the two LIGO facilities occurred in September 2015.[4] In August 2017 the European VIRGO detector joined the LIGO observation run.[5] The combined detection by three interferometers potentially improves the event localization from more than a thousand square degrees to tens of square degrees, depending of course on the strength of the signal.

The first EM counterpart of a GW event was observed on 17 August, 2017. This LIGO-VIRGO GW event[6]) was followed 1.7 s later by a short GRB (GRB 170817A) independently detected by the Fermi γ-ray Burst Monitor (GBM) and by IBIS on board INTEGRAL.[7] Many other facilities around the world started to search for the site of the event in all possible wavebands. It took approximately 11 hours before the source was identified in the lenticular galaxy NGC 4993.[8]

Increasing the number of simultaneously observed GW and EM counterparts is paramount to addressing fundamental questions on the nature of coalescing neutron stars and black-holes. The goal of the method

Further author information: (Send correspondence to R.R)
R.R.: E-mail: roir@campus.technion.ac.il

described in the present paper is to detect GRBs at high sensitivity and to identify their direction with high accuracy. Such capabilities will not only enable fast follow-up with telescopes, but will also allow LIGO-VIRGO to search for sub-threshold events once the time and direction are known.

1.2 GRB Localization

A single soft γ-ray detector unit generally cannot identify the direction of incident photons. Angular localization of GRBs thus require multiple detectors. The coded-mask aperture method, most successfully implemented on Swift-BAT,[9] is an array of detectors partially covered by a mask. The coded mask generates different shading patterns over the detectors array, varying with the source direction. This technique enables the reconstruction of the direction of a GRB up to 20' (minutes of arc). However, it requires a large detector area and volume due to the required separation between the mask and the array. Moreover, it has a limited field of view, and the mask blocks many of the source photons.

Another method is a sparse array of scintillators, e.g., on Compton-BATSE[10] and Fermi-GBM,[11] which are distributed over the spacecraft, each facing a different direction. The relative signals in each scintillator provide information about the direction of the source. For example, those facing the opposite direction are shielded by the satellite and will have lower count rates. Angular localization of soft γ-ray sources can also be achieved if the detectors are far enough apart, as on different space crafts, and the different times of arrival can be discriminated.[12] Alternatively, direction reconstruction is possible if the detection is time-coincident with another observation of a different messenger (e.g. visible light), where better angular accuracy is available.

2. THE GALI CONCEPT

In traditional astrophysical γ-ray detectors, scintillators are built with different cross-sections towards different directions to produce a gradually varying response with angle. These systems rely on the scintillators facing various orientations to reconstruct the direction of the source. In contrast, the γ-ray-burst Localizing Instrument (GALI) concept presented here exploits *mutual occultation* of numerous small scintillators, distributed within a small volume, to provide directional information. The method relies on the entire array looking significantly different from different directions. Due to the occultation, the count rates from each scintillator will vary dramatically as a function of the source direction, even for small angle differences. In a sense, this is similar to the coded mask aperture method, but the mask itself is composed of detecting scintillators, so that no precious photons are lost. The low count rates in each individual small scintillator are compensated by the large number of scintillators. As in traditional approaches, the sensitivity to weak sources depends on the total size of the detecting volume. Fig. 1 shows two prototype instruments demonstrating the differences between a traditional detector design and the present concept. The first is the Gamma ray Transient Monitor (GTM) whose design is similar to the Fermi/GBM, and which has been described in past SPIE proceedings.[13] The second is the GALI laboratory prototype described in section 4.2.

The GALI laboratory prototype presented here is composed of $(9\,\mathrm{mm})^3$ cubic scintillators. These are read out by Si Photo-Multipliers (SiPMs), which obviates the traditional, cumbersome, Photo-Multiplier Tubes (PMTs). Adopting such compact light sensors enables filling a volume with a large number of small detectors at the expense of the size of each individual one. An additional advantage of SiPMs over PMTs is their significantly lower operation voltage (tens of volt instead of hundreds).

A simulation of the system performance is presented in section 3, a detailed description of the experimental setup is given in section 4, and the results of the experiments are given in section 5.

3. SIMULATIONS

To check the performance of the GALI concept we run simulations using MEGAlib,[14] a simulation software based on Geant4.[15] In these simulations all γ-ray interactions with scintillators are considered as counts in the relevant scintillator. Each simulation run is composed of two steps: A bright GRB with no background and the background simulation. We use the bright GRB simulation to estimate the average counts on each scintillator in
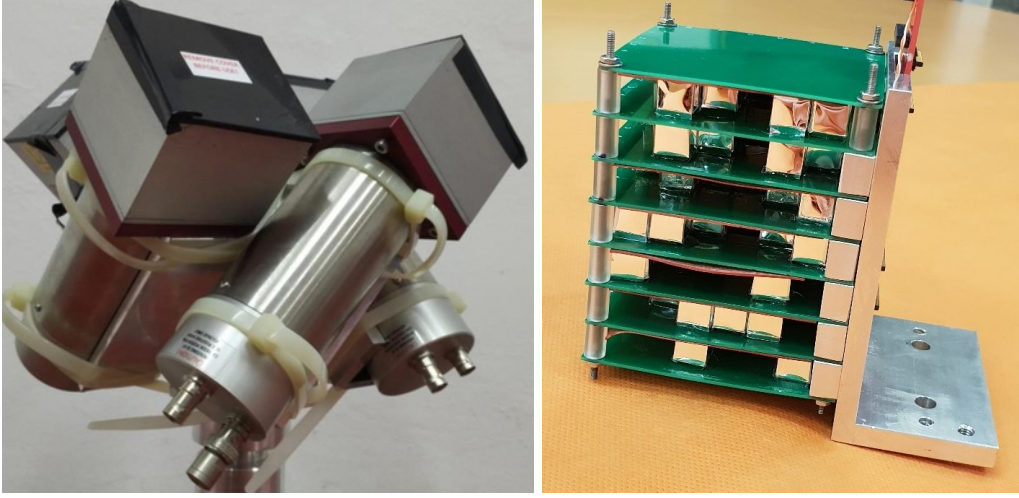
Figure 1: Two prototype instruments demonstrating the two conceptual detector designs **Left**: The GTM - a traditional design based on large, asymmetric box-shaped scintillators with various orientations. This design is similar to the Fermi/GBM. **Right**: The GALI design, which uses $(9\,\mathrm{mm})^3$ cubic scintillators in a 3D structure that exploits their different mutual occultation from different directions.

the system with no background: a burst of 1000 ph·cm^{-2} , whose photon spectrum (dN/dE) is a band function[16] (equation 1) with $\alpha = 1.1$, $\beta = 2.3$ and $E_{peak} = (2 + \alpha)E_0 = 266$ keV.

$$\frac{dN(E)}{dE} = A \begin{cases} (\frac{E}{100keV})^\alpha \exp\left(-\frac{E}{E_0}\right) & E \leq (\alpha - \beta)E_0 \\ \left[(\alpha - \beta)\frac{E_0}{100keV}\right]^{(\alpha-\beta)} (\frac{E}{100keV})^\beta \exp(\beta - \alpha) & E > (\alpha - \beta)E_0 \end{cases} \tag{1}$$

The simulations are repeated varying the angular coordinates at 5° intervals within the upper hemisphere. The average counts on each scintillator are then interpolated at either 0.5° or 1° intervals. We divide the average counts by the total number of counts for each burst to obtain the relative average counts on each scintillator. The result is an array of relative counts for each angle in the hemisphere. The background simulation is based on various lower earth orbit (LEO) observations of hard X-rays and γ-rays[17–21] and is included in the MEGAlib software package. Background caused by Leptonic and Hadronic components was not included, being estimated in simulation to be less than 1% of the photonic background, far less than the statistical uncertainty. The Hadronic background may need to be simulated later depending on the spacecraft platform which will host the experiment.

After running the simulations, we estimate the directional capabilities of the detector system. We consider 1 second bursts of 10 ph cm^{-2} s^{-1} from a given direction in the presence of the background. The burst is generated using the aforementioned relative average counts by applying poisson statistics to the expected average of each scintillator. We then add the background with poisson uncertainty. We reconstruct the burst direction using a cstat estimator[22] between the generated counts and the simulated ones at each angle. The reconstructed direction is that which gives minimal cstat value. The burst generation and direction reconstruction process is repeated 100 times for each angle at 5° intervals so as to generate an accuracy map of the entire hemisphere.

The simulated detectors are two different GALI systems: a random configuration of 90 $(9\,\mathrm{mm})^3$ scintillator cubes spread in a $6\times6\times7$ cm^3 volume and one of 350 cubes in a $10\times10\times10$ cm^3 volume. To compare the potential improvement of the GALI accuracy with respect to previous existing concepts, we also simulated the a GTM detector with four 3" diameter 1" thick cylindrical scintillators. The GTM has similar effective area compared to the 350-scintillator GALI, but has approximately twice that of the 90-scintillator GALI. The simulated systems are shown in figure 2. Notice that the 90-scintillator GALI contains the PCB boards upon which the detectors

are mounted as in the the lab prototype described in section 4.2, whereas no 350-scintillator GALI prototype exists, so no PCB boards have been included in this case.

A small sample of the generated bursts' direction reconstructed by the three systems is shown in figure 3. The all-sky average deviation of the reconstructed source direction from the original source direction in each system is 13.1° for the GTM, 6.5° for a 90-scintillator GALI and 1.7° for the 350-scintillator GALI. From these simulations we conclude that the localization accuracy of a system increases significantly with the number of detectors, even when the effective area of the entire system is reduced.
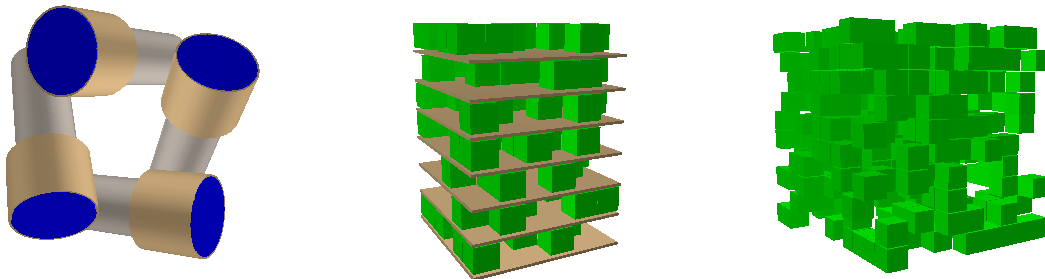

Figure 2: Three detector configurations compared using simulations. **Left**: A GTM configuration of four 3" diameter 1" thick cylindrical detectors - the GTM. **Middle**: A GALI configuration of ninety $(9\,mm)^3$ cubic scintillators. Between the detectors are PCB boards. This system is simulated as close as possible to a lab model. **Right**: A GALI configuration of 350 $(9\,mm)^3$ cubic scintillators.

4. EXPERIMENTAL SETUP

4.1 Individual detector unit characterization

We conducted a preliminary study to characterize single detector units in order to choose among different scintillating crystals, reflective wrappings and SiPM sensors. Each detector unit consists of a $(9\,mm)^3$ cubic scintillator wrapped or coated by a reflective material and coupled to a SiPM using Cargille Meltmount[*] optical glue, which has a refractive index of 1.7.

Scintillating crystals of two kinds were selected for their high density and light yield, as well as their negligible intrinsic radioactivity: CsI(Tl) (see for example Balamurugan et al.[23]) and Ce:GAGG.[24] Both scintillators were polished by and purchased from Advatek[†]. We coated the CsI(Tl) crystals by sputtering a 50 nm thick layer of SiO_2, which protects the delicate and slightly hygroscopic crystal from mechanical degradation and water absorption. Ce:GAGG suffers from afterglow for hours after exposure to light due to lattice defects;[25] therefore, it should be always kept in the dark so as not to alter the measurements. For space applications, the afterglow caused by electron and γ-ray dose needs to be considered.

γ-ray signals from our CsI(Tl) and Ce:GAGG crystals are read by a Sensl J60035 SiPM[‡] through a 10 kΩ resistor and recorded with an oscilloscope with 1 MΩ termination, and are shown in figure 4. In these measurements the SiPM was operated at a 27.2 V bias. The recorded voltage pulse is a convolution of the SiPM response function and the scintillation time evolution.[26] For both crystals in the present configuration (RC∼40 μs, given C∼4 nF) the scintillation time is shorter than the circuit typical decay time. Therefore, the measured voltage is

---

[*] https://www.cargille.com/mounting-media

[†] https://www.advatech-uk.co.uk

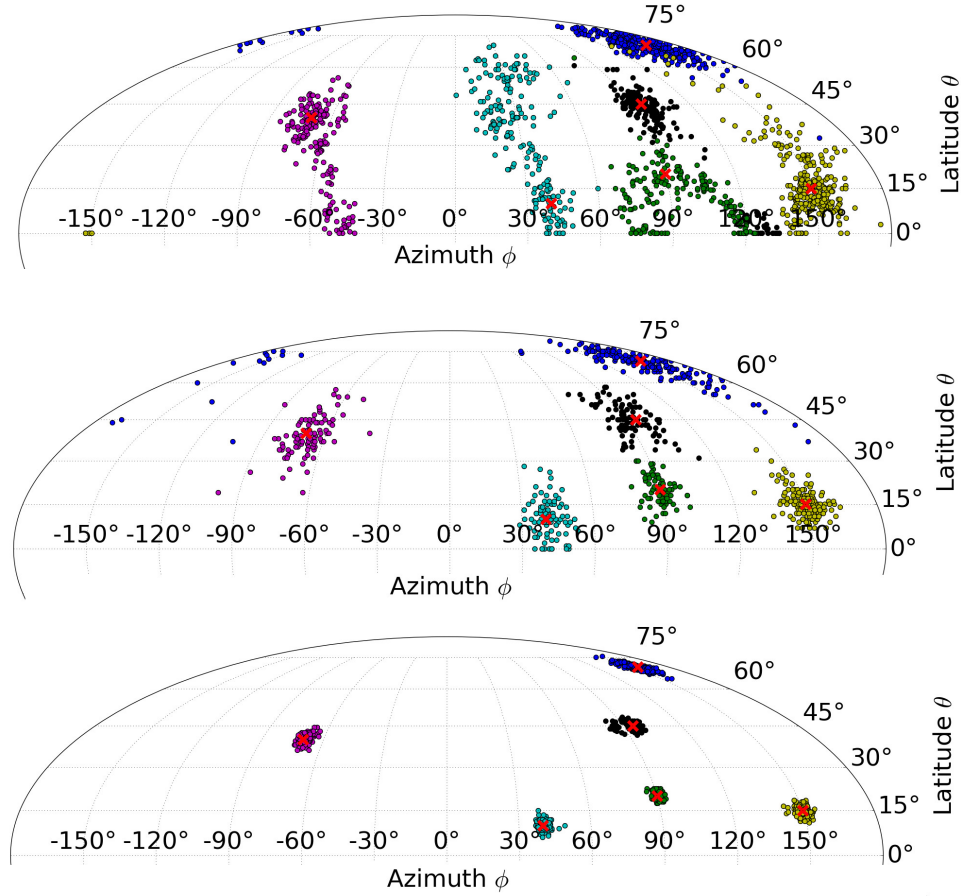[‡] https://www.onsemi.com/pub/Collateral/MICROJ-SERIES-D.PDF

Figure 3: A comparison between the simulation-generated GRBs direction reconstructed by different detector configurations. Each dot represents a 1 s burst of 10 ph cm^{-2} s^{-1} at lower earth orbit. Dots are grouped by color according to the actual burst direction, which is represented by a × mark. **Top**: GTM. **Middle**: 90-scintillator GALI. **bottom**: 350-scintillator GALI. Notice the clear improvement in localization accuracy when the number of scintillators is increased.

proportional to the integrated charge produced by the SiPM, and the peaks in figure 4 corresponds to the end of the scintillation light production. The voltage recovery follows the circuit RC value. Figure 4b shows the full Ce:GAGG light emission signal, which presents a fast component (∼100 ns) and a slow tail (ending at ∼500 ns) that can be distinguished by the signal slope change. In the same figure it can be seen that the CsI(Tl) light emission is much slower than the Ce:GAGG one. During the 500 ns in which the Ce:GAGG emission is completed, CsI(Tl) produces only ∼40% of the total charge. In figure 4a the full CsI(Tl) signal is shown, reaching its maximum value within ∼6 μs. Most existing integrated readout electronics have much shorter integration times, which may hinder the sensitivity of CsI(Tl) scintillators. Considering a readout electronics having ∼1 μs integration time (like the TOFPET2 ASICs described in section 4.2) there is a clear advantage in using Ce:GAGG for better signal-to-noise.

We measured charge spectra produced by the two crystals using an Ortec 671 spectroscopy amplifier with an Ortec Aspec-927 MCA. We set the amplifier shaping time to 0.5 μs for Ce:GAGG and to 3 μs for CsI(Tl) to include the full signal rise. The latter value is due to the signal shortening because of the low input impedance (465 Ω) of the amplifier. Spectra from a ^{137}Cs source from both scintillators are presented in figure 5. The ratio of the number of counts in the 662 keV peak between the two scintillators is ∼2 in favor of Ce:GAGG, whereas for the 32 keV peak the ratio is comparable (taking into account the higher Compton baseline of Ce:GAGG). This indicates a higher detection efficiency of Ce:GAGG due to its higher density. On the other hand, it has
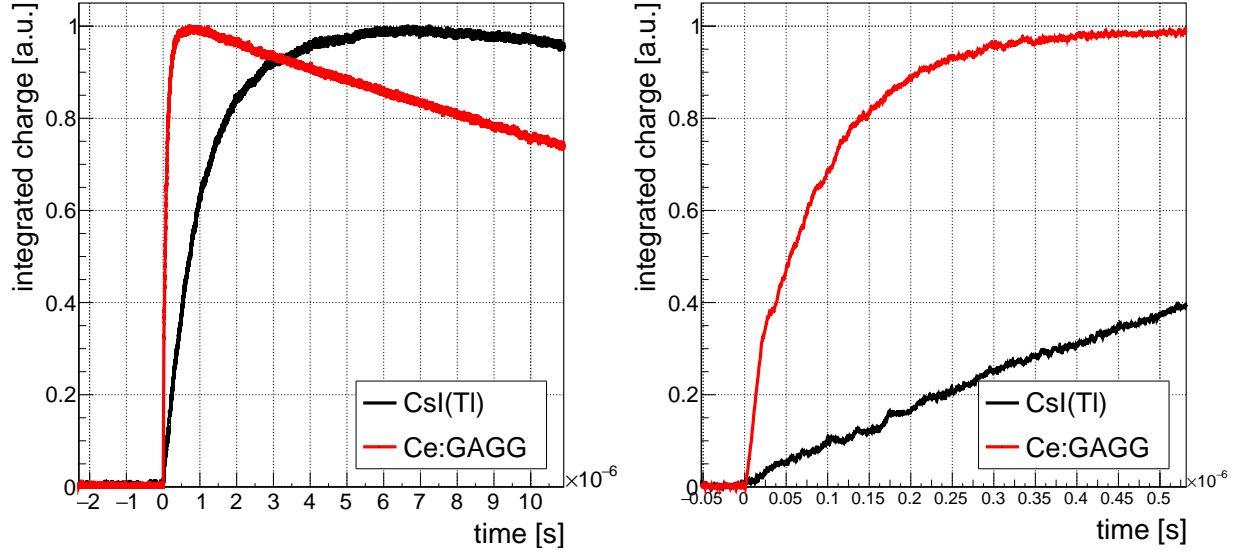
Figure 4: γ-ray signals from CsI(Tl) and Ce:GAGG crystals read by a SiPM coupled to ground through a 10 kΩ resistor. The right hand side shows the first 500 ns of the plot on the left. The measured voltage is proportional to the integrated charge produced by the SiPM. The peak corresponds to the end of the light production, which is faster for Ce:GAGG. The voltage recovery follows the circuit RC value.

been reported[27] that at low energies CsI(Tl) provides ∼120% response with respect to the response at high energy while Ce:GAGG provides only ∼85%. In conditions in which the signal to noise ratio is low, such as high temperature or high SiPM dark count rates (for example due to radiation damage), the noise threshold rises, so the advantage due to higher Ce:GAGG efficiency can be jeopardized. In general, the spectra peak positions result from a few factors: the crystal light yield, the SiPM gain and the effect of the amplifier. Investigating these factors and their γ-ray energy dependence requires a dedicated study with multiple radioactive sources, which is beyond the scope of the present study.

Based on the presented results we conclude that there might be advantages in choosing Ce:GAGG for its faster light emission and higher detection efficiency. Despite that, for our first system prototype we chose CsI(Tl) because of its lower cost. Next we plan to build a full Ce:GAGG prototype to compare their performance.

The SiPM models that we considered are: Sensl J60035 and Hamamatsu 14160-6050HS[28][§]. The most relevant features for the two kinds are summarized in table 4.1. The Sensl J60035 SiPM has two clear advantages: a 13.5 V lower breakdown voltage and a smaller cell size, which implies a linear response until higher gamma energies. On the other hand, Hamamatsu 14160-6050HS has lower dark current, which is important for space applications. Additionally, according to vendor data the Hamamatsu 14160-6050HS has a ∼10% enhanced PDE in the region above 450 nm, where the emission of both scintillators peaks.

Type	size	V_{bd}[V]	max I_{dark}[μA]	cell size [μm]	capacitance [nF]
Sensl J60035	6 mm	24.5	12	35	4
Hamamatsu 14160-6050HS	6 mm	38	7.5	50	2

Another important parameter for space applications is radiation hardness, meaning capability to withstand doses of highly ionizing particles with an acceptable performance degradation. We could not find any study
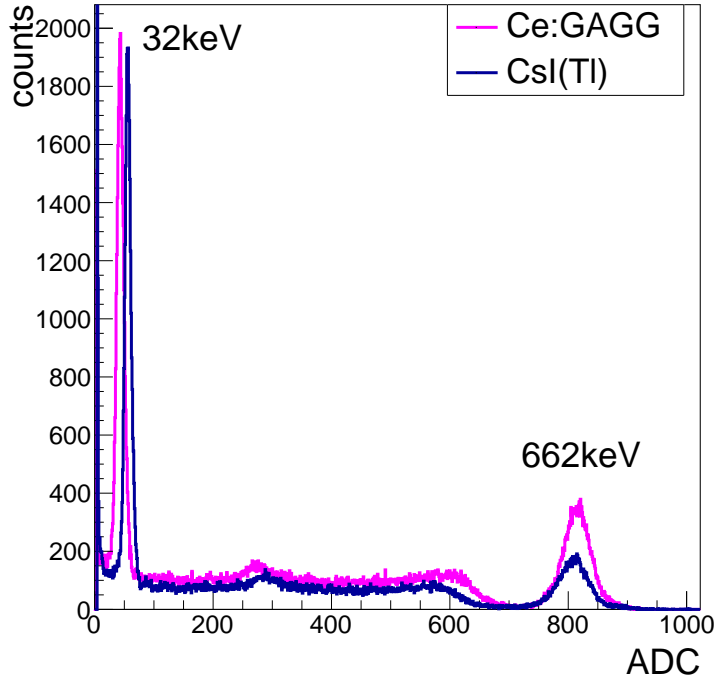
Figure 5: Spectra from a ^{137}Cs source detected by $(9\,\text{mm})^3$ CsI(Tl) and Ce:GAGG cubic scintillators. The 662 keV peaks clearly show the higher detection efficiency of Ce:GAGG at high energies.

of performance degradation due to intense irradiation for Sensl J60035, whereas recent studies were published for Hamamatsu 14160-6050HS within the context of the CAMELOT mission.[29] One study shows that for Hamamatsu 14160-6050HS the performance degradation - in terms of dark current and noise threshold - due to 200 MeV protons recovers over time, as it undergoes an annealing process at room temperature.[30] Another study reports that heavy-ion irradiation causes an increased dark current and a worse energy resolution, but the effect is overall mild.[31]

Clearly, more testing of radiation damage on SiPM is required. Nonetheless, taking all this into account we chose Hamamatsu 14160-6050HS for our prototype.

Reflective materials of various kinds can be applied to the crystal faces in order to maximize the light collection from the crystal to the SiPM. The reflectors considered here are: Teflon tape (diffusive), Ag-Al coating (specular), and 3M-Vikuiti^{TM} enhanced specular reflector (ESR).

The Teflon tape is 80 μm thick and needs to be winded a few times around the crystal, which is glued onto the SiPM, as shown in figure 6a. We discarded Teflon wrapping because of its large thickness and the difficulty of applying it uniformly and repeatably in the same fashion for each unit.

We sputtered SiO$_2$-coated CsI(Tl) crystals with a 200 nm Ag layer and then a more robust 200 nm Al layer on top of it. A 6 mm square area at the center of one cube face was left open to couple the SiPM. An example of such a unit is shown in figure 6b.

The Vikuiti ESR is a 65 μm thick film. It was laser-cut and glue[¶] was applied to specific areas to keep it closed after folding. The wrapping process is illustrated in figure 7.
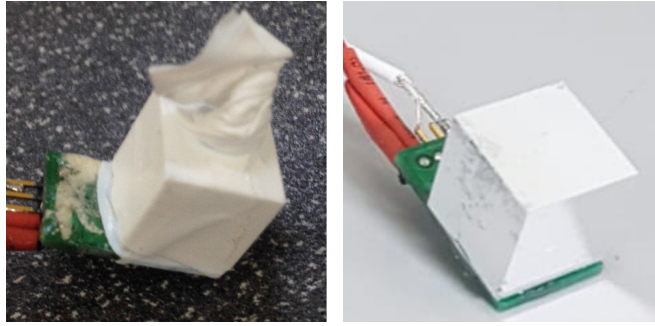

[¶]3M-9471

Figure 6: **Left:** A CsI(Tl) crystal coupled to a SiPM and then wrapped in Teflon tape. **Right:** A CsI(Tl) crystal coated with Al and Ag and coupled to a SiPM.

Figure 7: From left to right, the CsI(Tl) crystal wrapping process with Vikuiti ESR.

A comparison of a ^{137}Cs spectrum measured by a CsI(Tl) crystal coated with Ag and Al with one measured by a Vikuiti ESR wrapped crystal is presented in figure 8. From the ratio of the 662 keV peaks position, one can see that the light transport in the coated crystal results in a ∼2.2 times lower signal than the Vikuiti ESR wrapped one. This is surprising, given the fact that both Ag and Al have a reflectivity higher than 90% in the CsI(Tl) spectral range. This effect deserves further investigation. Since we repeated a similar experiment with a Ce:GAGG crystal obtaining similar results, we conclude that the cause is probably not a chemical reaction that alters the properties of the surface. For Vikuiti ESR wrapping there is a layer of air between the crystal and the reflector which causes internal reflection to take place. This may affect the results, but it is not clear if this fact alone can explain the significant difference from the coated crystal.

4.2 GALI detector prototype

Our first GALI prototype is a system of 90 detector units assembled in the way described in section 4.1. Each CsI(Tl) crystal is coated with SiO_2, wrapped in Vikuiti ESR film and coupled to a Hamamatsu 14160-6050HS SiPM with optical glue. The detector units are arranged on 7 layers of standard FR4 PCB boards, each hosting 13 or 12 units. First, the SiPMs are soldered onto the PCBs, then the wrapped crystals are glued to them by means of a positioning jig. During the gluing stage the PCB and the glue dispenser are kept in an oven so that the glue melts. An assembled layer is shown in figure 9a. The layers are then stacked by means of poly-carbonate rods and spacers and aluminium holders that allow mounting the entire stack on motorized axes for automatic angle scanning. On the back of the vertical axis a PETSys DAQ system is mounted[‖]: a scalable readout based on the TOFPET2 ASICs. Each detector layer is connected to one of the two ASICs front-end boards through a PCB adapter. The front-end boards are connected to the DAQ through flat cables. Each ASIC has 64 channels independently connected to a single SiPM. On top of providing bias voltage to the SiPM,
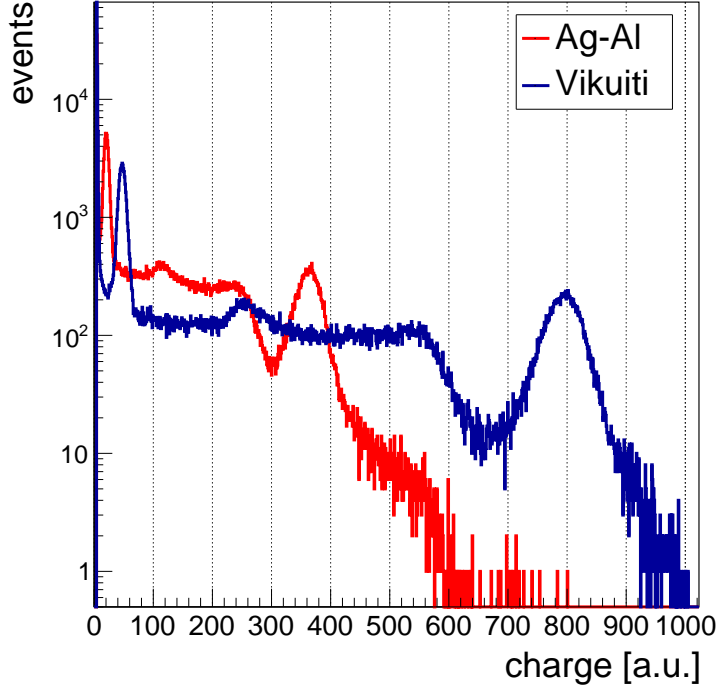

[‖]https://www.petsyselectronics.com

Figure 8: Comparison of a ^{137}Cs spectrum measured by a CsI(Tl) crystal coated with Ag and then Al, and one measured by a Vikuiti ESR wrapped crystal. The light transport in the coated crystal results in noticeably less charge.

each channel integrates its output current and digitizes the integral whenever a threshold value is passed. The raw data are stored conveniently in a ROOT** tree for offline analysis. The data acquisition software can be controlled by python†† scripts, as well as the rotating axes, so that the measurements are fully automated.

The entire assembly is shown in figure 9b. We installed the assembly in a thermally insulating dark box where back-fed peltier plates keep the inner temperature constant at 24±0.5°C. This is crucial for a stable gain of the SiPMs and of the DAQ.

5. LOCALIZATION MEASUREMENTS AND RESULTS

In order to test the direction reconstruction capabilities of GALI we expose it to a 10 mCi ^{241}Am source placed approximately 3.5 meters away to simulate a distant source. The effective flux of the 59.6 keV line at this distance is approximately 50 ph cm^{-2} s^{-1}. We scan the entire hemisphere by varying θ between 0 and 90° and ϕ between 0 and 360° with 5° intervals. For each angle we acquire two kinds of measurements. First a 60 s long exposure (corresponding to up to $\sim$ 3000 counts on each scintillator), and then a series of 100 bursts 0.5 s long. Measurements are analyzed offline. We use the long measurements to define the spectrum region of interest for each detector unit, namely, 2σ region around the 59.6 keV Gaussian peak. The long measurements also provide the average counts in each detector at each angle. These are then interpolated at 0.5° intervals. We then test the GALI direction reconstruction accuracy of the bursts, similar to the method described for the simulations (section 3).

To quantify the advantages of the new concept, we compare GALI to the traditional design used in the GTM. The results of the 90-scintillator GALI are compared to those obtained by a GTM prototype composed of four

---

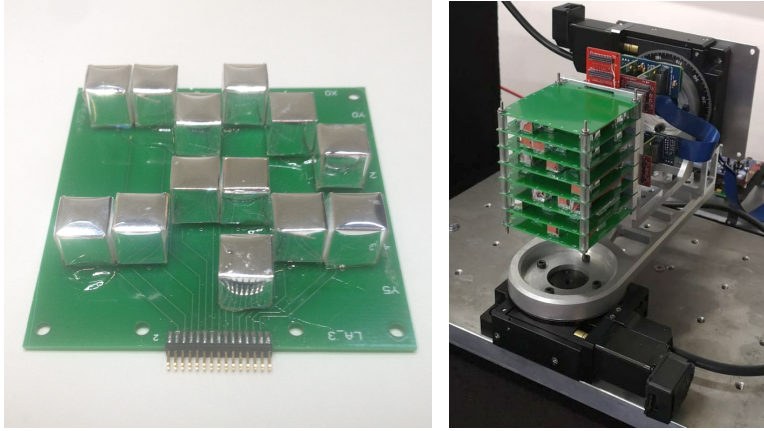**https://root.cern.ch

††https://www.python.org

Figure 9: **Left:** A GALI detector layer composed of 13 units assembled on a PCB board. **Right:** The present prototype, equipped with PETSys DAQ system. The assembly is installed on motorized axes, which allows automatic angle scanning.

6.35×6.35×2.54 cm^3 box NaI scintillators. For practical reasons the GTM experiment is limited to a quarter of the hemisphere. The GTM system is exposed to the source for 30 s. Due to the larger effective area of each scintillator, a 30 s exposure (corresponding to $\gtrsim$ 50000 counts on each scintillator), is enough to establish the reference average counts. We Test the GTM localization capabilities using 50 bursts of $\sim 0.5 \pm 0.05$ s. This uncertainty in burst length is caused by limitations of the DAQ system (CAEN DT5724[‡‡]). The GTM data are analyzed in a similar manner to the GALI data as described above.

A comparison between the performance of the GTM system and the 90-scintillator GALI is shown in figure 10 for 12 different burst directions. As can be seen, the 90-scintillator system demonstrates better accuracy overall. The average error for the shown reconstructed bursts ranges between 1.3° and 2.8° for the 90-scintillator GALI and between 3° and 21° for the GTM. GALI performs strictly better in all measured directions. The improvement in accuracy is often greater than 50%, despite the significantly smaller total detecting volume of GALI with respect to the GTM.

6. CONCLUSIONS

The present experiments can be summarized as follows

- We present a novel directional GRB detector concept based on mutual occultation of numerous, small scintillator elements.

- For this purpose, we explored both CsI(Tl) and Ce:GAGG scintillators, as well as their coating and wrapping procedures. Two SiPM readout elements were also compared. We chose for the current experiment to use CsI(Tl) coated with SiO_2 and wrapped by a Vikuiti ESR reflector.

- We built a laboratory prototype consisting of 90 CsI(Tl) (9 mm)^3 cubes stacked in 7 layers. Relative count rates were measured at angles over the entire hemisphere with long (60 s) exposures, and used as reference. Subsequently, the direction reconstruction capability was tested on short bursts (0.5 s).

- Experimental results with the 59.6 keV peak of ^{241}Am show that short bursts ($\sim$25 ph cm^{-2}) can be localized to within 1°–3°.

- Simulations of a 350-scintillator instrument, including true LEO background and GRB spectra, show an accuracy of $\sim 1.7°$, which outperforms any existing scintillator-based GRB instrument that we are aware of, including much bigger ones.
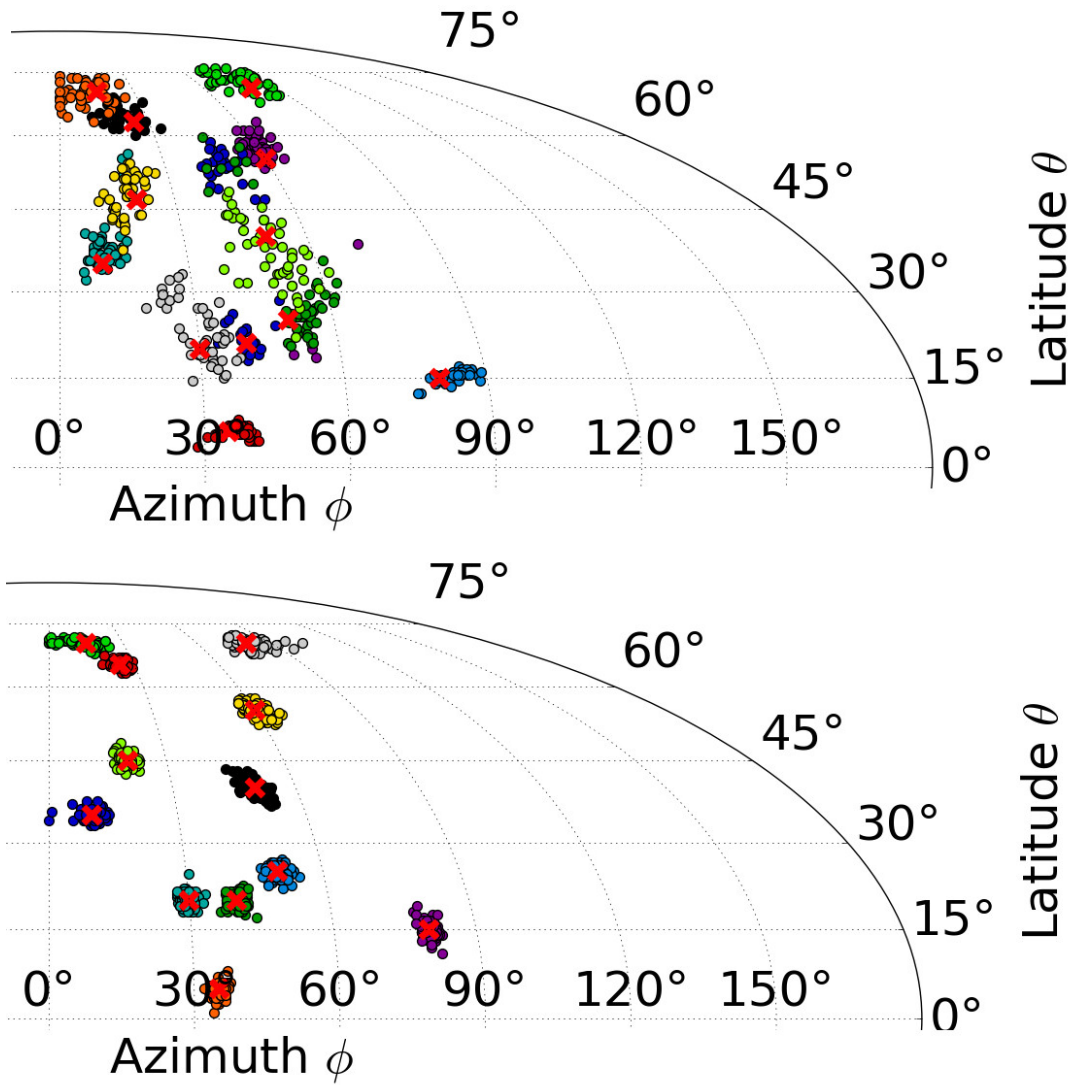

[‡‡]https://www.caen.it

Figure 10: A comparison between laboratory tests of the GTM (**Top**) and a 90-scintillator GALI (**Bottom**). The reconstructed direction of repeated 0.5 s bursts are plotted where each dot represents a burst. Dots are grouped by color according to the actual source direction, which is represented by a × mark. Confirming the simulations, the superior angular localization accuracy of GALI is clear.

ACKNOWLEDGMENTS

REFERENCES

[1] Blinnikov, S. I., Novikov, I. D., Perevodchikova, T. V., and Polnarev, A. G., "Exploding neutron stars in close binaries," *Pisma v Astronomicheskii Zhurnal* **10**, 422–428 (June 1984).

[2] Paczynski, B., "Gamma-ray bursters at cosmological distances," *The Astrophysical Journal* **308**, L43–L46 (1986).

[3] Mochkovitch, R., Hernanz, M., Isern, J., and Martin, X., "Gamma-ray bursts as collimated jets from neutron star/black hole mergers," *Nature* **361**(6409), 236–238 (1993).

[4] Abbott, B. P., Abbott, R., Abbott, T., Abernathy, M., Acernese, F., Ackley, K., Adams, C., Adams, T., Addesso, P., Adhikari, R., et al., "Observation of gravitational waves from a binary black hole merger," *Physical review letters* **116**(6), 061102 (2016).

[5] Abbott, B. P., Abbott, R., Abbott, T., Acernese, F., Ackley, K., Adams, C., Adams, T., Addesso, P., Adhikari, R. X., Adya, V., et al., "Gw170814: a three-detector observation of gravitational waves from a binary black hole coalescence," *Physical review letters* **119**(14), 141101 (2017).

[6] Abbott, B. P., Abbott, R., Abbott, T., Acernese, F., Ackley, K., Adams, C., Adams, T., Addesso, P., Adhikari, R., Adya, V., et al., "Gw170817: observation of gravitational waves from a binary neutron star inspiral," *Physical Review Letters* **119**(16), 161101 (2017).

[7] Abbott, B. P., Abbott, R., Abbott, T., Acernese, F., Ackley, K., Adams, C., Adams, T., Addesso, P., Adhikari, R., Adya, V., et al., "Gravitational waves and gamma-rays from a binary neutron star merger: Gw170817 and grb 170817a," *The Astrophysical Journal Letters* **848**(2), L13 (2017).

[8] Abbott, B. P., Collette, C., et al., "Multi-messenger observations of a binary neutron star merger," *Astrophysical Journal. Letters* **848**(2), L12 (2017).

[9] Barthelmy, S. D., Barbier, L. M., Cummings, J. R., Fenimore, E. E., Gehrels, N., Hullinger, D., Krimm, H. A., Markwardt, C. B., Palmer, D. M., Parsons, A., et al., "The burst alert telescope (bat) on the swift midex mission," *Space Science Reviews* **120**(3-4), 143–164 (2005).

[10] Fishman, G. J., Meegan, C. A., Parnell, T. A., Wilson, R. B., Paciesas, W., Mateson, J. L., Cline, T. L., and Teegarden, B. J., "Burst and Transient Source Experiment (BATSE) for the Gamma Ray Observatory (GRO)," in [*19th International Cosmic Ray Conference (ICRC19), Volume 3*], *International Cosmic Ray Conference* **3**, 343–346 (Aug. 1985).

[11] Meegan, C., Lichti, G., Bhat, P., Bissaldi, E., Briggs, M. S., Connaughton, V., Diehl, R., Fishman, G., Greiner, J., Hoover, A. S., et al., "The fermi gamma-ray burst monitor," *The Astrophysical Journal* **702**(1), 791 (2009).

[12] Fiore, F., Burderi, L., Salvo, T. D., Feroci, M., Labanti, C., Lavagna, M. R., and Pirrotta, S., "HERMES: a swarm of nano-satellites for high energy astrophysics and fundamental physics," in [*Space Telescopes and Instrumentation 2018: Ultraviolet to Gamma Ray*], den Herder, J.-W. A., Nikzad, S., and Nakazawa, K., eds., **10699**, International Society for Optics and Photonics, SPIE (2018).

[13] Yacobi, L., Abramov, R., Lupu, N., Vdovin, A., Kaidar, A., Rahin, R., Feigenboim, A., Levine, B. M., Osovizky, A., Camp, J., Tarem, S., and Behar, E., "The gamma-ray transient monitor for ISS-TAO: new directional capabilities," in [*Space Telescopes and Instrumentation 2018: Ultraviolet to Gamma Ray*], den Herder, J.-W. A., Nikzad, S., and Nakazawa, K., eds., **10699**, 1417 – 1424, International Society for Optics and Photonics, SPIE (2018).

[14] Zoglauer, A., Andritschke, R., and Schopper, F., "Megalib–the medium energy gamma-ray astronomy library," *New Astronomy Reviews* **50**(7-8), 629–632 (2006).

[15] Agostinelli, S., Allison, J., Amako, K. a., Apostolakis, J., Araujo, H., Arce, P., Asai, M., Axen, D., Banerjee, S., Barrand, G. ., et al., "Geant4—a simulation toolkit," *Nuclear instruments and methods in physics research section A: Accelerators, Spectrometers, Detectors and Associated Equipment* **506**(3), 250–303 (2003).

[16] Band, D., Matteson, J., Ford, L., Schaefer, B., Palmer, D., Teegarden, B., Cline, T., Briggs, M., Paciesas, W., Pendleton, G., et al., "Batse observations of gamma-ray burst spectra. i-spectral diversity," *The Astrophysical Journal* **413**, 281–292 (1993).

[17] Gruber, D., Matteson, J., Peterson, L., and Jung, G., "The spectrum of diffuse cosmic hard x-rays measured with heao 1," *The Astrophysical Journal* **520**(1), 124 (1999).

[18] Mizuno, T., Kamae, T., Godfrey, G., Handa, T., Thompson, D., Lauben, D., Fukazawa, Y., and Ozaki, M., "Cosmic-ray background flux model based on a gamma-ray large area space telescope balloon flight engineering model," *The Astrophysical Journal* **614**(2), 1113 (2004).

[19] Ajello, M., Greiner, J., Sato, G., Willis, D., Kanbach, G., Strong, A., Diehl, R., Hasinger, G., Gehrels, N., Markwardt, C., et al., "Cosmic x-ray background and earth albedo spectra with swift bat," *The Astrophysical Journal* **689**(2), 666 (2008).

[20] Abdo, A., Ackermann, M., Ajello, M., Atwood, W., Baldini, L., Ballet, J., Barbiellini, G., Bastieri, D., Baughman, B., Bechtol, K., et al., "Fermi large area telescope observations of the cosmic-ray induced γ-ray emission of the earth's atmosphere," *Physical Review D* **80**(12), 122004 (2009).

[21] Türler, M., Chernyakova, M., Courvoisier, T.-L., Lubiński, P., Neronov, A., Produit, N., and Walter, R., "Integral hard x-ray spectra of the cosmic x-ray background and galactic ridge emission," *Astronomy & Astrophysics* **512**, A49 (2010).

[22] Cash, W., "Parameter estimation in astronomy through application of the likelihood ratio," *The Astrophysical Journal* **228**, 939–947 (1979).

[23] Balamurugan, N., Arulchakkaravarthi, A., Selvakumar, S., Lenin, M., Kumar, R., Muralithar, S., Sivaji, K., and Ramasamy, P., "Growth and characterization of undoped and thallium doped cesium iodide single crystals," *Journal of crystal growth* **286**(2), 294–299 (2006).

[24] Kamada, K., Yanagida, T., Endo, T., Tsutumi, K., Usuki, Y., Nikl, M., Fujimoto, Y., Fukabori, A., and Yoshikawa, A., "2 inch diameter single crystal growth and scintillation properties of ce: Gd3al2ga3o12," *Journal of Crystal Growth* **352**(1), 88–90 (2012).

[25] Yoneyama, M., Kataoka, J., Arimoto, M., Masuda, T., Yoshino, M., Kamada, K., Yoshikawa, A., Sato, H., and Usuki, Y., "Evaluation of gagg: Ce scintillators for future space applications," *Journal of Instrumentation* **13**(02), P02023 (2018).

[26] Spanoudaki, V. C. and Levin, C. S., "Scintillation induced response in passively-quenched si-based single photon counting avalanche diode arrays," *Optics express* **19**(2), 1665–1679 (2011).

[27] Sibczynski, P., Broslawski, A., Gojska, A., Kiptily, V., Korolczuk, S., Kwiatkowski, R., Mianowski, S., Moszyński, M., Rzadkiewicz, J., Swiderski, L., et al., "Characterization of some modern scintillators recommended for use on large fusion facilities in γ-ray spectroscopy and tomographic measurements of γ-emission profiles," *Nukleonika* **62**(3), 223–228 (2017).

[28] Yamamoto, K., Nagano, T., Yamada, R., Ito, T., and Ohashi, Y., "Recent development of mppc at hamamatsu for photon counting applications," in [*Proceedings of the 5th International Workshop on New Photon-Detectors (PD18)*], 011001 (2019).

[29] Řípa, J., Galgóczi, G., Werner, N., Pál, A., Ohno, M., Mészáros, L., Mizuno, T., Tarcai, N., Torigoe, K., Uchida, N., et al., "Estimation of the detected background by the future gamma ray transient mission camelot," *Astronomische Nachrichten* **340**(7), 666–673 (2019).

[30] Hirade, N., Takahashi, H., Uchida, N., Ohno, M., Torigoe, K., Fukazawa, Y., Mizuno, T., Matake, H., Hirose, K., Hisadomi, S., Nakazawa, K., Yamaoka, K., Werner, N., Řípa, J., Hatori, S., Kume, K., and Mizushima, S., "Annealing of proton radiation damages in Si-PM at room temperature," *Nuclear Instruments and Methods in Physics Research A* **986**, 164673 (Jan. 2021).

[31] Link, J. T., Akaike, Y., Binns, W., Bose, R., Brandt, T., Buckley, J., Cannady, S., De Nolfo, G., Dowkontt, P., Du Monthier, J., et al., "Silicon Photomultiplier use in Particle Astrophysics and Heliophysics Missions," in [*36th International Cosmic Ray Conference (ICRC2019)*], *International Cosmic Ray Conference* **36**, 96 (July 2019).